Supplementary information

Viral lysing can alleviate microbial nutrient limitations and accumulate recalcitrant dissolved organic matter components in soil

Di Tong[a,b], Youjing Wang [a,b], Haodan Yu [a,b], Haojie Shen [a,b], Randy A. Dahlgren [c], Jianming Xu [a,b*]

[a]Institute of Soil and Water Resources and Environmental Science, College of Environmental and Resource Sciences, Zhejiang University, Hangzhou 310058, China

[b]Zhejiang Provincial Key Laboratory of Agricultural Resources and Environment, Zhejiang University, Hangzhou 310058, China

[c]Department of Land, Air and Water Resources, University of California, Davis, CA, USA

*Corresponding author. E-mail: jmxu@zju.edu.cn.

Supplementary Materials and Methods

1. Analysis of extracellular enzyme activity and putative microbial physiological traits

Extracellular enzymes related to the degradation of organic carbon (β-1,4-glucosidase [BG], cellobiohydrolase [CBH]), nitrogen (β-1,4-N-acetyl-glucosaminidase [NAG] and L-leucine aminopeptidase [LAP]), and phosphorus (acid phosphatase [AP]) were quantified within 48 h of sample collection by fluorometric methods [1-3]. Briefly, 1 g soil was homogenized with 125 mL acetate buffer (50 mM, pH 5.0) and stirred vigorously for 2 h using a magnetic stir plate. Then, 50 μL of soil slurry mixed with 100 μL fluorometric substrate solution (200 μmol L^{-1}) and 50 μL acetate buffer were incubated at 25 °C for 4 h, in the dark. The reaction was stopped by adding a 10 μL aliquot of 1.0 M NaOH. A multifunctional microplate reader was used to measure fluorescence at 365 nm excitation and 450 nm emission wavelengths and expressed in the unit of nmol h^{-1} g^{-1} [4].

The lengths and angles of enzymatic vectors can be used to illustrate relative microbial resource acquisition strategies [4-5]. Vector length and angle were calculated as:

$$V_{length} = SQRT(x^2 + y^2) \quad (1)$$

$$V_{angle}\ (degree) = Degrees\left(Atan2(x, y)\right) \quad (2)$$

In these functions, x represents the relative activities of C vs. P acquiring enzymes ([BG + CBH]/[BG + CBH + AP]) and y represents the relative activities of C vs. N acquiring enzymes ([BG + CBH]/[BG + CBH + NAG + LAP]). SQRT signifies the square root of the sum of the squared values of x and y, and Atan2 represents the four-quadrant inverse tangent.

2. Calculation of microbial metabolic efficiency

Microbial metabolic efficiency can be represented by qCO_2 and CUE, where higher metabolic efficiency equates to lower qCO_2 and higher CUE [6]. Soil qCO_2 signifies microbial respiration per unit biomass and is expressed in the units of mg CO_2–C mg^{-1} MBC d^{-1} [7]. According to the biogeochemical equilibrium model, CUE was indirectly calculated as equations (3-5).

$$CUE = CUE_{max} \times \sqrt{\frac{S_{C:N} \times S_{C:P}}{(K_{C:N}+S_{C:N}) \times (K_{C:P}+S_{C:P})}} \quad (3)$$

$$S_{C:N} = B_{C:N}/L_{C:N} \times 1/EEA_{C:N} \quad (4)$$

$$S_{C:P} = B_{C:P}/L_{C:P} \times 1/EEA_{C:P} \quad (5)$$

Where $EEA_{C:N}$ and $EEA_{C:P}$ were calculated as ln(BG)/ln(NAG + LAP) and ln(BG)/ln(AP), respectively. $L_{C:X}$ is the molar C:X ratio of labile substrates (e.g., labile carbon, nitrogen and phosphorus represented by DOC, inorganic N (NH_4^+ + NO_3^-) and available P, respectively). $B_{C:X}$ is the molar ratio of microbial biomass carbon, nitrogen

and phosphorus. According to thermodynamic constraints of the saturating Michaelis-Menten formulation, CUE_{max} represents the maximum microbial growth efficiency, and was set as 0.60. $K_{C:X}$ was fixed to 0.50 and represents the half-saturation constant [6].

Supplementary Figures

Figure S1. Cumulative CO_2 fluxes during incubation at 25℃ (A) and 15℃ (B).

Figure S2. Cumulative CO_2 emission for incubations at three time points of 7 d (A, B), 28 d (C, D) and 98 d (E, F).

Figure S3. Calculation of Q_{10} (mean ±std dev) at different groups.

Figure S4. Metabolic quotient (qCO_2, respiration per unit of microbial biomass, mg CO_2–C mg^{-1} MBC d^{-1}).

Figure S5. Microbial resource acquisition strategy.

Figure S6. Excitation-emission matrix (A, B, C) of DOM for three fluorescent components.

Figure S7. Hydrophobicity of DOM after incubation as determined by SUV260.

Figure S8. Correlation heatmap between microbial resource acquisition traits and optical properties of DOM.

Figure S9. Principal coordinates analysis (PCoA) of bacterial communities in different groups at incubation temperatures of 25 ℃ (A) and 15 ℃ (B).

Figure S10. Redundancy analysis (RDA) at OTU level demonstrating the effect of soil physicochemical properties on bacterial communities for different groups.

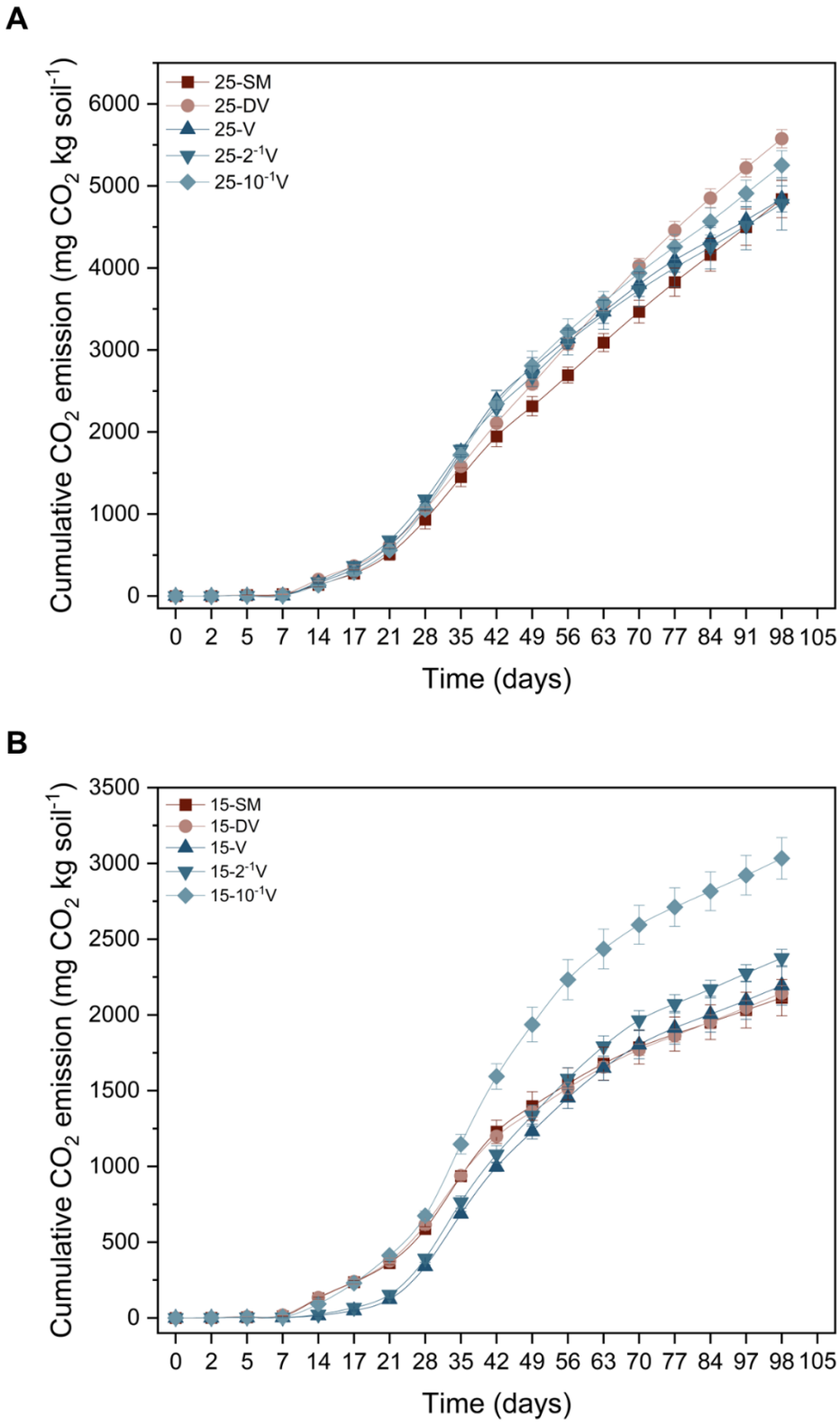

Figure S1. Cumulative CO_2 fluxes (mean ±std dev) during incubation at 25 ℃ (A) and 15 ℃ (B). SM, no added viruses; DV, added-inactive viruses; V, added-active viruses

with no dilution; 2^{-1} V, added-active viruses with 2-fold dilution; 10^{-1} V, added-active viruses with 10-fold dilution; 25 and 15 signify temperature (25℃ and 15℃) during the incubation.

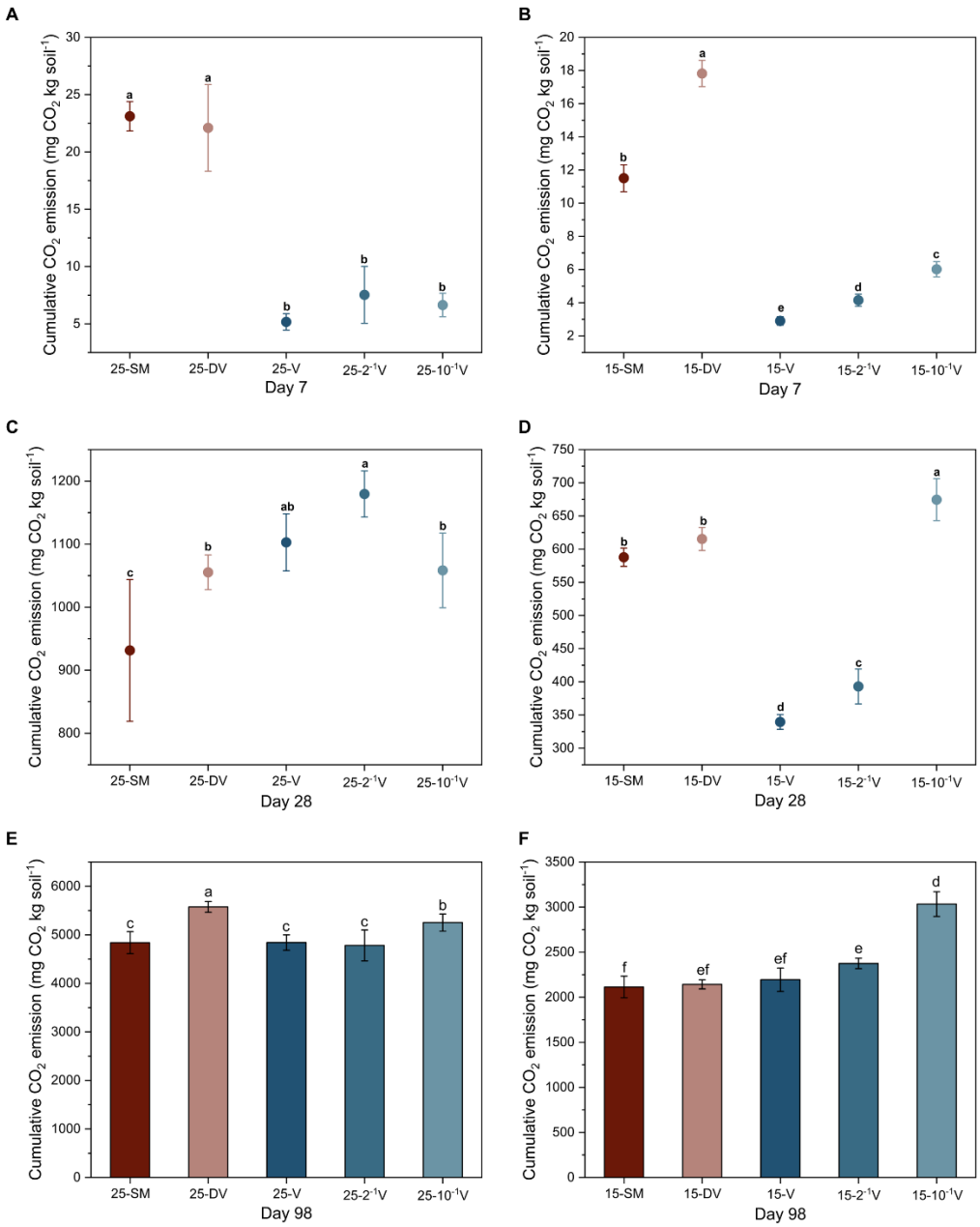

Figure S2. Cumulative CO_2 emission (mean ±std dev) for incubations at three time points of 7 d (A, B), 28 d (C, D) and 98 d (E, F). SM, no added viruses; DV, added-inactive viruses; V, added-active viruses with no dilution; 2^{-1} V, added-active viruses with 2-fold dilution; 10^{-1} V, added-active viruses with 10-fold dilution; 25 and 15 signify temperature (25°C and 15°C) during the incubation. Different lowercase letters

represent significant differences at $p < 0.05$.

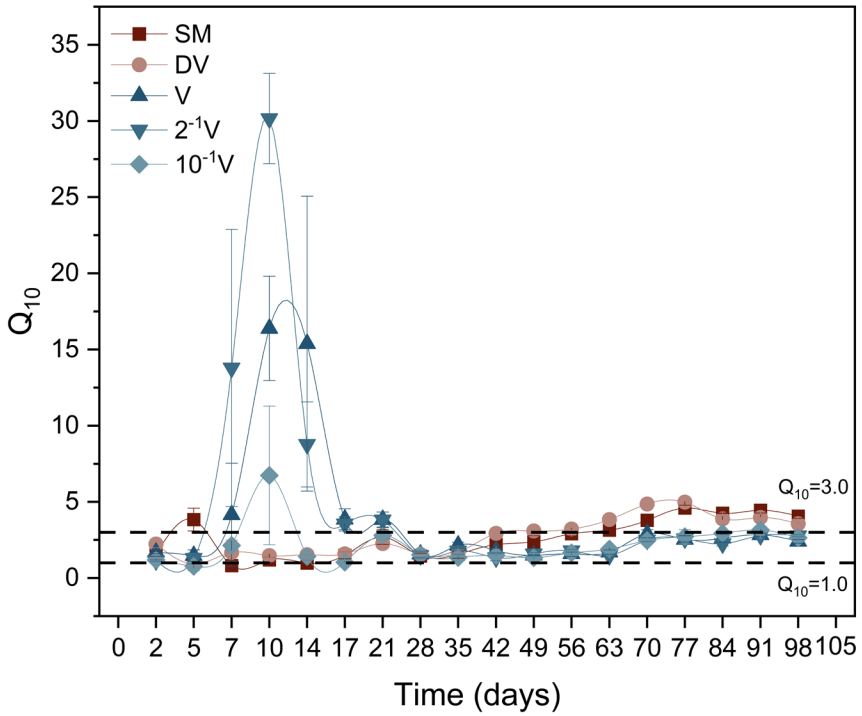

88

89 **Figure S3.** Calculation of Q_{10} (mean ±std dev) at different groups. SM, no added viruses;

90 DV, added-inactive viruses; V, added-active viruses with no dilution; 2^{-1} V, added-active

91 viruses with 2-fold dilution; 10^{-1} V, added-active viruses with 10-fold dilution.

92

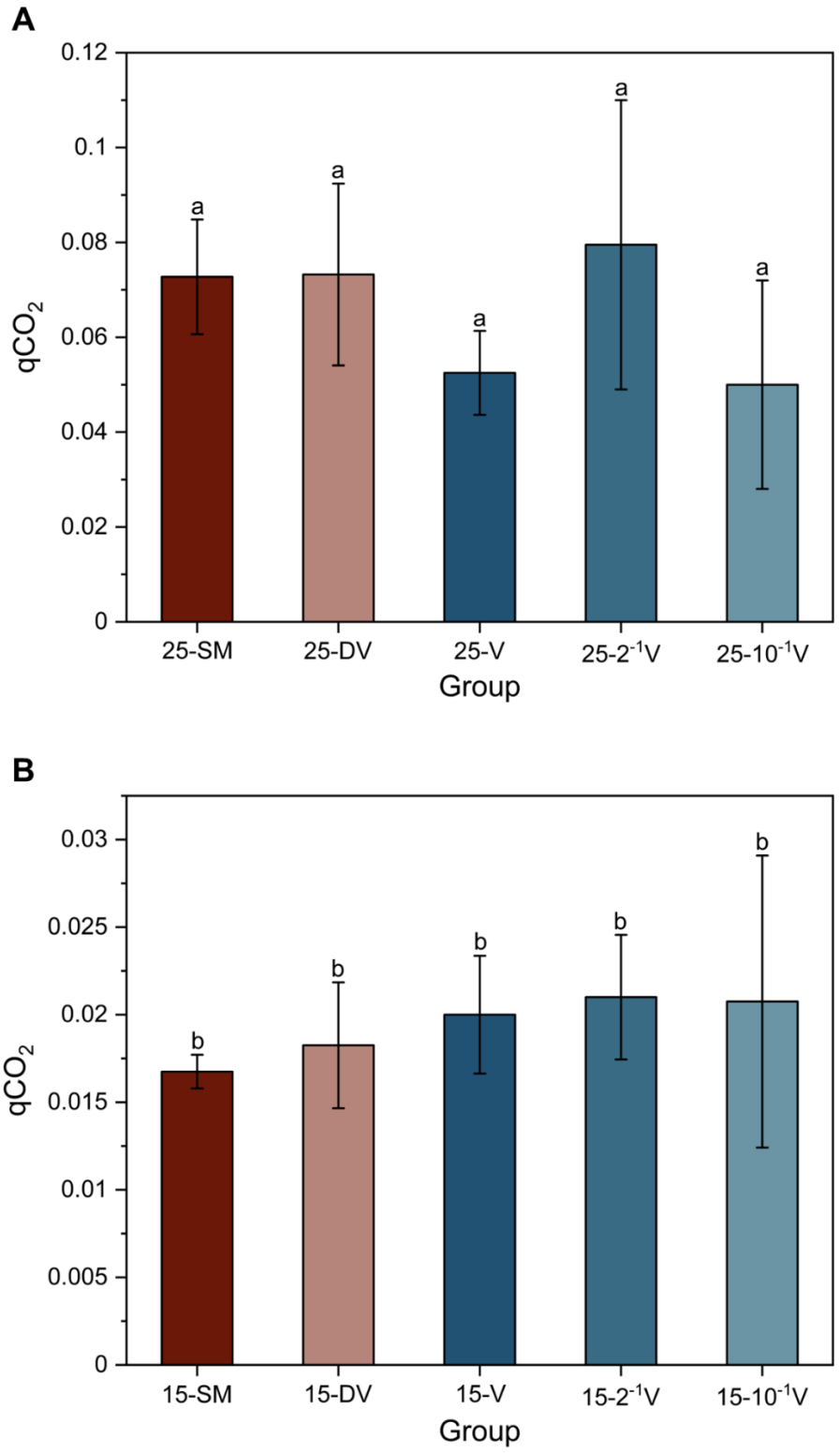

Figure S4. Metabolic quotient (mean ±std dev; qCO_2, respiration per unit microbial biomass, mg CO_2–C mg^{-1} MBC d^{-1}). SM, no added viruses; DV, added-inactive viruses;

V, added-active viruses with no dilution; 2^{-1} V, added-active viruses with 2-fold dilution; 10^{-1} V, added-active viruses with 10-fold dilution; 25 and 15 signify the temperature (25 ℃ and 15 ℃) during the incubation. Different lowercase letters represent significant differences at $p < 0.05$.

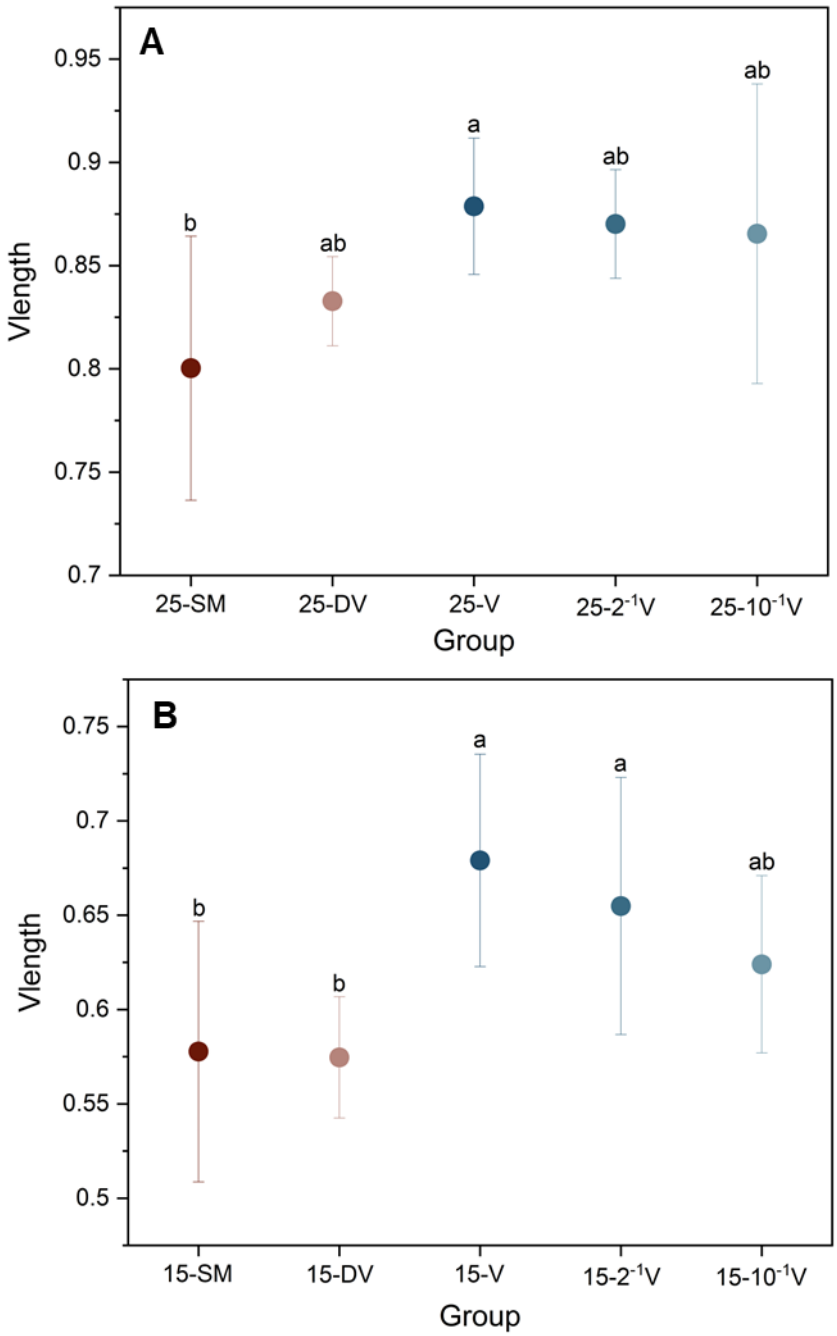

Figure S5. Microbial resource acquisition strategy (mean ±std dev). The Length quantified the relative C vs. nutrient (N and P)-acquiring enzyme activities. A lower Length indicates relatively higher nutrient acquisition strategies (relative to C). SM, no added viruses; DV, added-inactive viruses; V, added-active viruses with no dilution; 2^{-}

[1] V, added-active viruses with 2-fold dilution; 10^{-1} V, added-active viruses with 10-fold dilution; 25 and 15 signify the temperature (25 ℃ and 15 ℃) during the incubation. Different lowercase letters represent significant differences at $p < 0.05$.

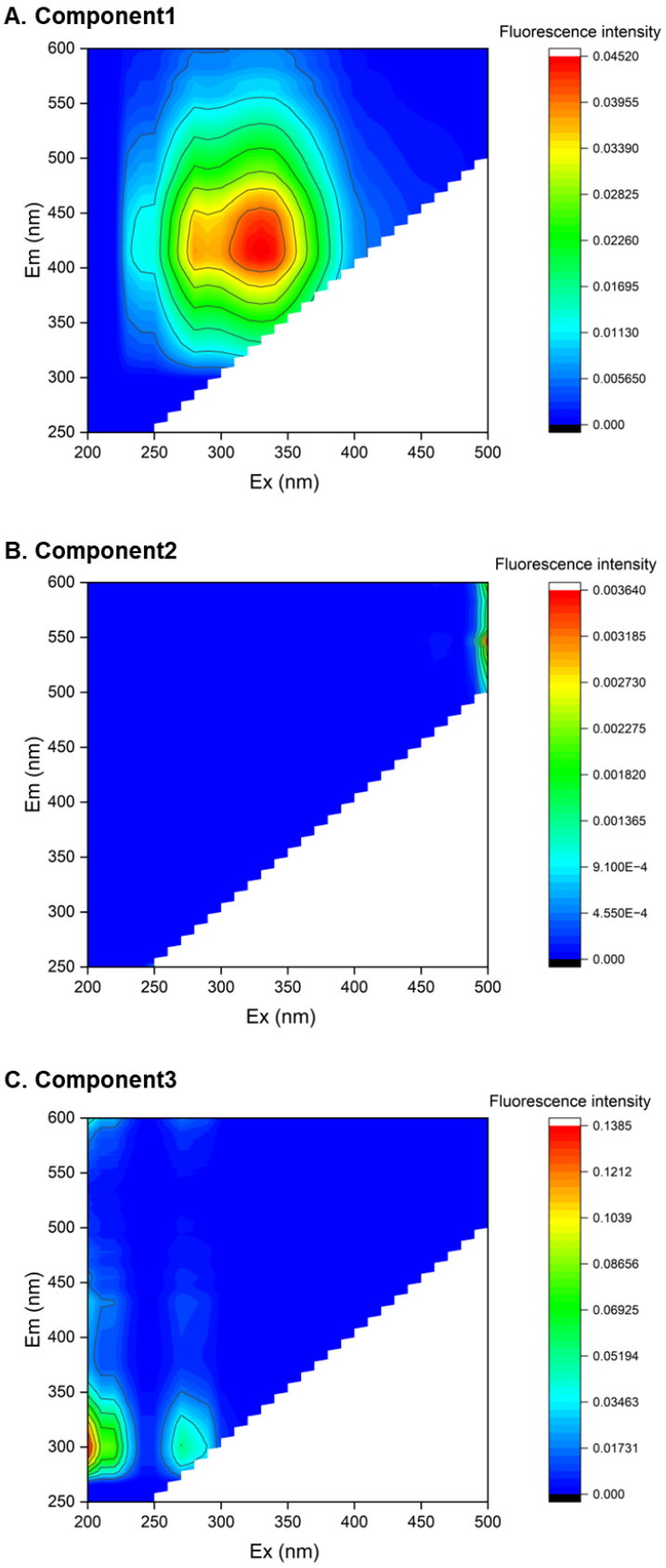

110

111 **Figure S6.** Excitation-emission matrix (A, B, C) of DOM for three fluorescent

components (Component 1: humic-like components [8-9]; Component 2: quinone-like components [10]; Component 3: protein-like component [11]) identified by EEM-PARAFAC analysis.

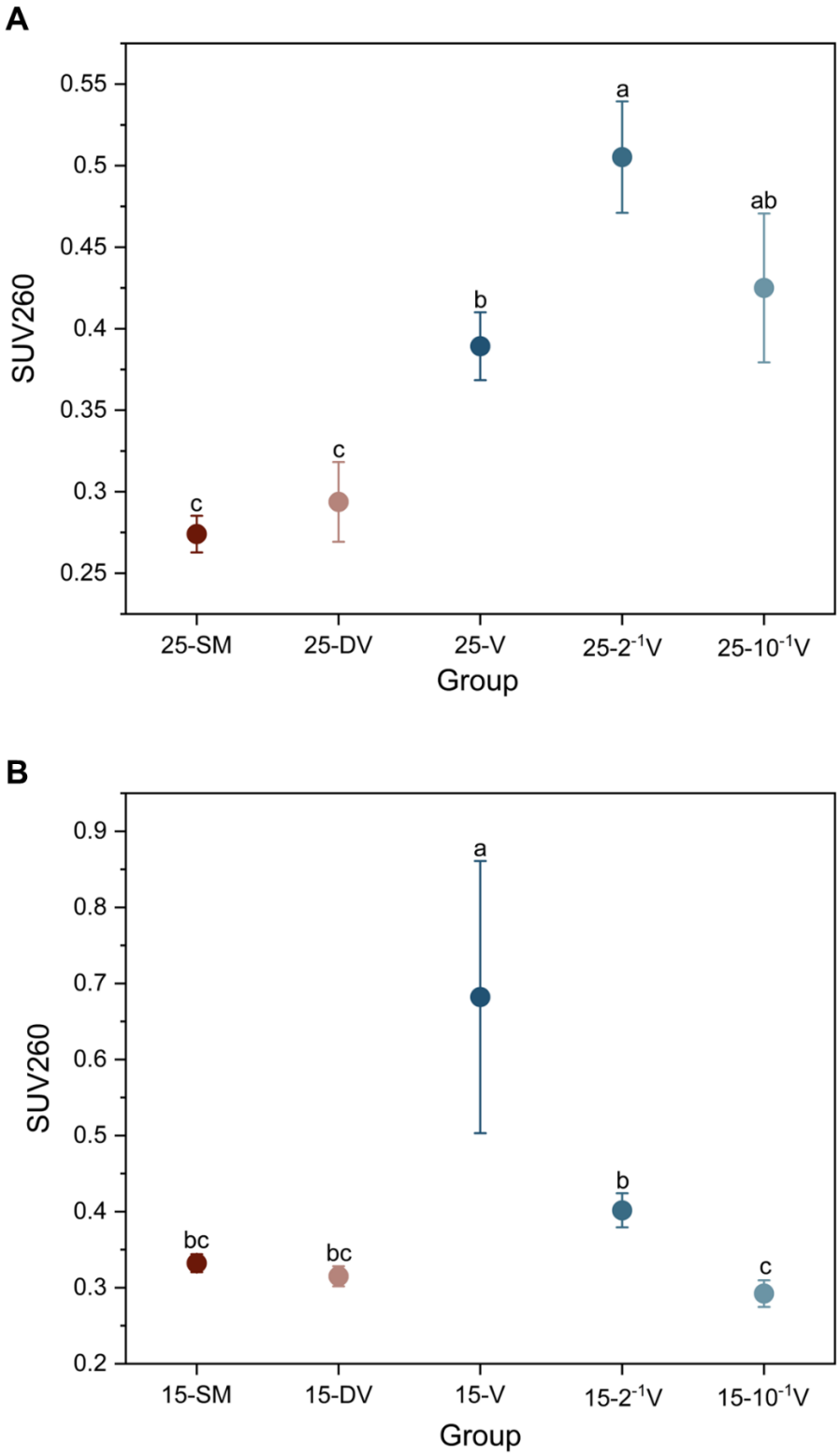

Figure S7. Hydrophobicity of DOM after incubation (mean ±std dev) as determined by SUV260. SM, no added viruses; DV, added-inactive viruses; V, added-active viruses

with no dilution; 2^{-1} V, added-active viruses with 2-fold dilution; 10^{-1} V, added-active viruses with 10-fold dilution; 25 and 15 signify the temperature (25 ℃ and 15 ℃) during the incubation. Different lowercase letters represent significant differences at $p < 0.05$.

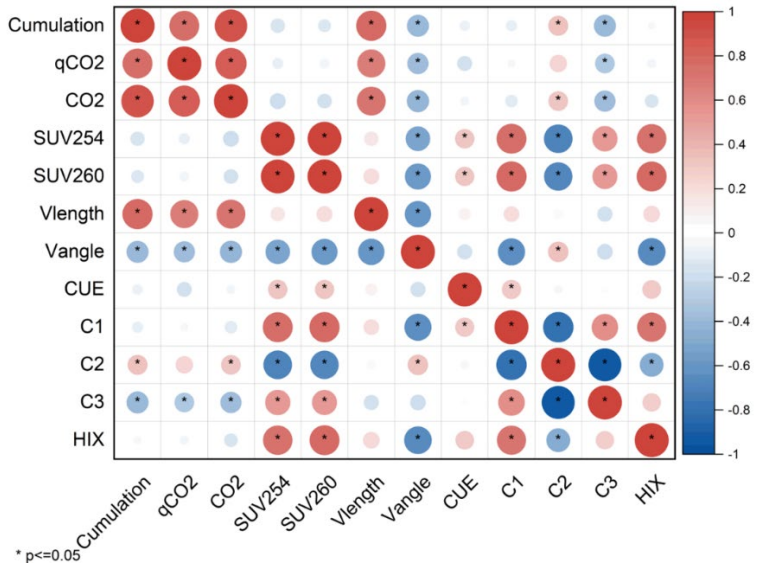

124

125 **Figure S8.** Correlation heatmap between microbial resource acquisition traits and

126 optical properties of DOM. Cumulation, cumulative CO_2 emission; qCO_2, metabolic

127 quotient, CUE, carbon use efficiency; CO_2, the CO_2 emission rate; HIX, aromaticity

128 degree of DOM; C1 (humic-like), C2 (quinone-like), and C3 (protein-like), different

129 3D-fluorescence components of DOM; SUV254, represents the humification of DOM;

130 SUV260, represents the hydrophobicity of DOM; Length, relative C:nutrient acquiring

131 ratio; Angle, relative P:N-acquiring ratio.

132

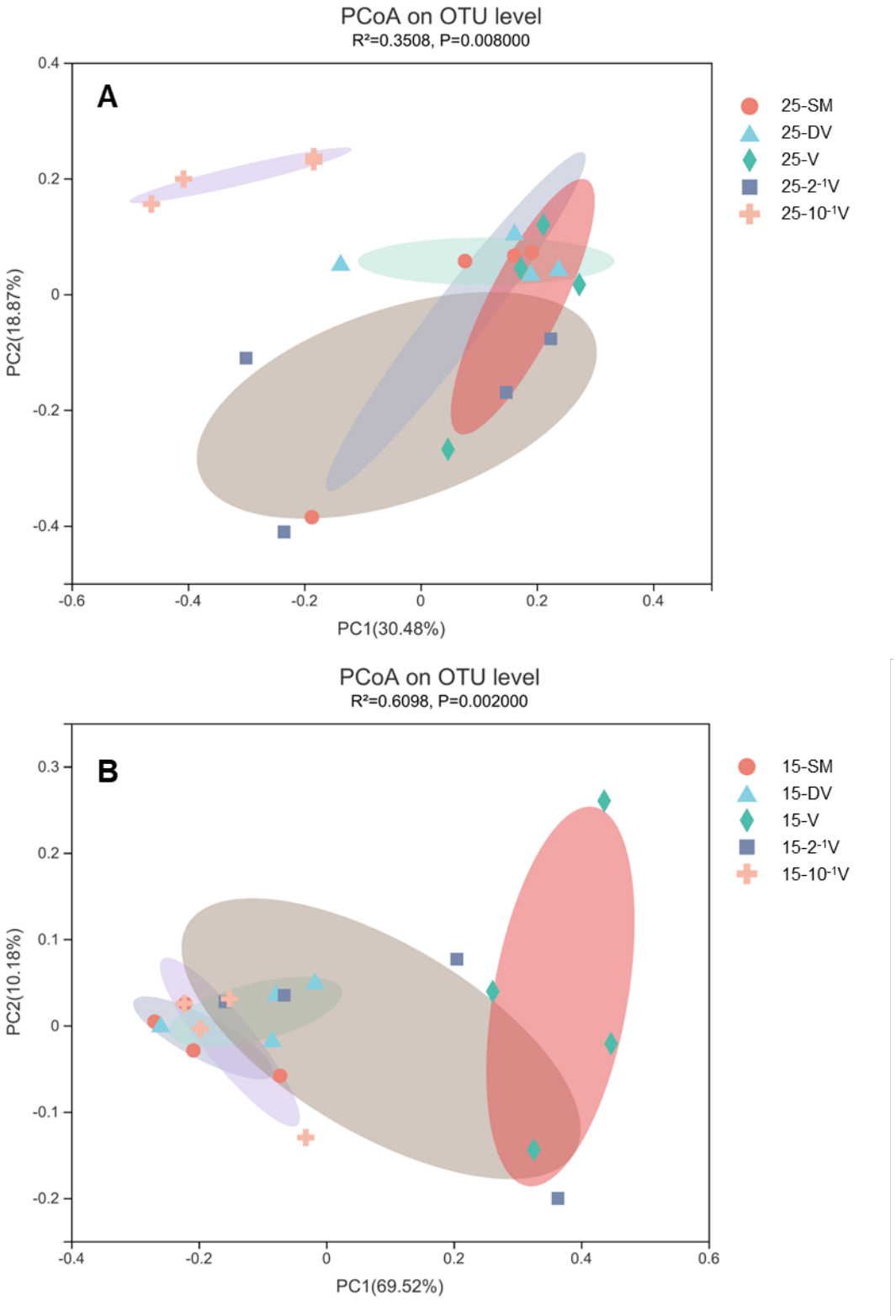

Figure S9. Principal coordinates analysis (PCoA) of bacterial communities in different groups at incubation temperatures of 25 ℃ (A) and 15 ℃ (B).

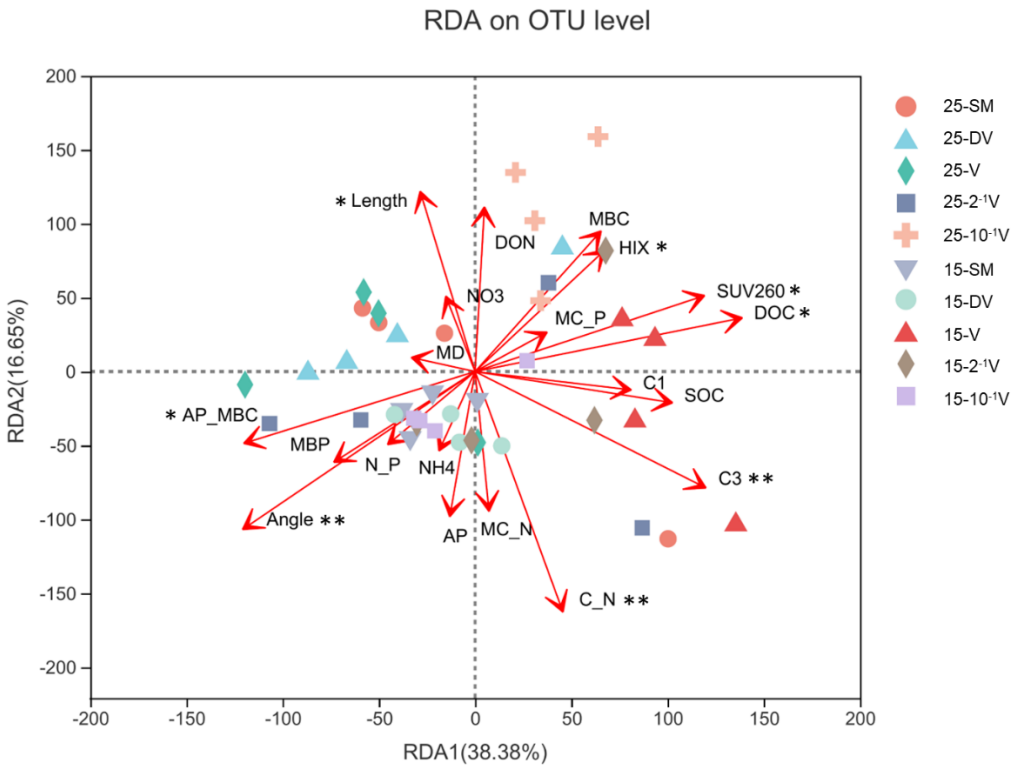

Figure S10. Redundancy analysis (RDA) at OTU level demonstrating the effect of soil physicochemical properties on bacterial communities for different groups. NO3, soil nitrate-N; NH4, soil ammonium-N; AP, available phosphorus; SOC, soil organic carbon; TN, total nitrogen; DOC, dissolved organic carbon; DON, dissolved organic nitrogen; N/P, the mass ratio of total nitrogen and total phosphorus; C/P, the mass ratio of soil organic carbon and total phosphorus; C/N, the mass ratio of soil organic carbon and total nitrogen; AP/MBC represents normalized enzyme activities of acid phosphatase as units/mg MBC; Ecoenzymatic vector length (length, relative C:nutrient acquiring ratio) and angle (angle, relative P:N-acquiring ratio); HIX, aromaticity degree of DOM; C1 (humic-like), C3 (protein-like), different 3D-fluorescence components of

DOM; MD, relative molecular mass of DOM; SUV260, hydrophobicity of DOM; MBC, microbial biomass carbon; MBP, microbial biomass phosphorus. *$p < 0.05$; **$p < 0.01$.

References:

1. Zheng H, Vesterdal L, Schmidt IK, Rousk J. Ecoenzymatic stoichiometry can reflect microbial resource limitation, substrate quality, or both in forest soils. Soil Biol Biochem. 2022;167:108613.

2. Li B, Li Y, Fanin N, Han X, Du X, Liu H, et al. Adaptation of soil micro-food web to elemental limitation: evidence from the forest-steppe ecotone. Soil Biol Biochem. 2022;170:108698.

3. Saiya-Cork KR, Sinsabaugh RL, Zak DR. The effects of long term nitrogen deposition on extracellular enzyme activity in an *Acer saccharum* forest soil. Soil Biol Biochem. 2002;34:1309-15.

4. Cui Y, Fang L, Guo X, Han F, Ju W, Ye L, et al. Natural grassland as the optimal pattern of vegetation restoration in arid and semi-arid regions: evidence from nutrient limitation of soil microbes. Sci Total Environ. 2019;648:388-97.

5. Moorhead DL, Sinsabaugh RL, Hill BH, Weintraub MN. Vector analysis of ecoenzyme activities reveal constraints on coupled C, N and P dynamics. Soil Biol Biochem. 2016;93:1-7.

6. Feng J, Zeng X-M, Zhang Q, Zhou X-Q, Liu Y-R, Huang Q. Soil microbial trait-based strategies drive metabolic efficiency along an altitude gradient. ISME Commun. 2021:71.

7. Dong L, Li J, Zhang Y, Liu Y, Li A, Shangguan Z, et al. Forests have a higher soil C sequestration benefit due to lower C mineralization efficiency: evidence from the central loess plateau case. Agric Ecosyst Environ. 2022;339:108144.

8. Brogi SR, Cossarini G, Bachi G, Balestra C, Camatti E, Casotti R, et al. Evidence of Covid-19 lockdown effects on riverine dissolved organic matter dynamics

provides a proof-of-concept for needed regulations of anthropogenic emissions. Sci Total Environ. 2022;812:152412.

9. Ren W, Wu X, Ge X, Lin G, Zhou M, Long Z, et al. Characteristics of dissolved organic matter in lakes with different eutrophic levels in southeastern Hubei Province, China. Chin J Oceanol Limnol. 2021;39:1256-76.

10. Cory RM, McKnight DM. Fluorescence spectroscopy reveals ubiquitous presence of oxidized and reduced quinones in dissolved organic matter. Environ Sci Technol. 2005;39:8142-49.

11. Gao Z, Gueguen C. Distribution of thiol, humic substances and colored dissolved organic matter during the 2015 Canadian Arctic GEOTRACES cruises. Mar Chem. 2018;203:1-9.